



# Deep Learning-Based Identification of High-Risk Zones for Lumpy Skin Disease in Cattle

**G Ramasubba Reddy<sup>1</sup> . Shaik Jaffar Hussain<sup>2</sup> . Penubaka Balaji<sup>3</sup> . L Jayasree<sup>4</sup> .  
 K Divya<sup>5</sup> . M Sudhakara<sup>6</sup>**

<sup>1</sup>Department of Computer Science and Engineering, Sai Rajeswari Institute of Technology, Proddatur, Andhra Pradesh, India.

<sup>2</sup>Department of Computer Science and Engineering, Sri Venkateswara Institute of Science and Technology, Kadapa.

<sup>3</sup>Department of Computer Science and Engineering, K L University, Vaddeswaram, Guntur, Andhra Pradesh, India.

<sup>4</sup>Dept of Computer Science and Engineering, Sri Padmavati Mahila Visva Vidyalayam, Tirupati - 517 502, AP, India.

<sup>5</sup>Department of Computer Science and Engineering, Narayana Engineering College, Nellore, Andhra Pradesh.

<sup>6</sup>Senior Computer Vision Scientist, ChiStats Labs Private Limited, Pune.

DOI: **10.5281/zenodo.15005382**

Received: 18 February 2025 / Revised: 07 March 2025 / Accepted: 10 March 2025

©Milestone Research Publications, Part of CLOCKSS archiving

**Abstract** – Lumpy skin disease (LSD) is a virus infection in cattle, mainly transmitted through mosquitoes, such as blood-eating insects. The disease creates essential challenges for the livestock industry by affecting milk and beef production and domestic and international trade. Resource limitations, lack of specialized expertise, and lack of time often obstruct traditional clinical approaches. This study introduces a deep learning-based framework for segmenting and classifying LSD-affected skin regions to address these challenges. The proposed approach leverages a 10-layer Convolutional Neural Network (CNN) trained on a curated Cattle Lumpy Skin Disease (CLSD) dataset. The significance of skin discoloration in disease identification is that a color histogram enhances feature extraction. The segmented affected regions undergo further processing through a deep pre-trained CNN for feature extraction, followed by threshold-based binarization. Finally, classification is performed using an Extreme Learning Machine (ELM) classifier, achieving an accuracy of 96% on the CLSD dataset. Comparative analysis with existing



state-of-the-art techniques demonstrates the effectiveness of the proposed methodology, highlighting its potential for reliable LSD diagnosis in cattle.

**Index Terms** – Lumpy Skin Disease (LSD), Cattle Disease Diagnosis, Deep Learning, Convolutional Neural Networks (CNN), Image Segmentation, Color Histogram, Extreme Learning Machine (ELM), CLSD Dataset, Livestock Health Monitoring.

## I. INTRODUCTION

Mostly affecting cattle, lumpy skin disease (LSD) is a contagious virus spread by blood-feeding insects like mosquitoes [1]. This illness poses a severe danger to the worldwide livestock sector, which supports livelihoods and food security and accounts for over 40% of the value of agricultural output [2]. Sustaining cattle health is crucial for both economic viability and global food security [3]. Due to its rapid cross-border spread, LSD poses a significant threat, especially in regions with warm, humid climates that support the establishment of disease-carrying arthropods. Reduced milk and meat output, trade restrictions, and financial losses for cow owners are only a few of the significant adverse economic repercussions of LSD [4]. Herbal remedies and manual cauterization are examples of traditional treatment methods still commonly used in many places, particularly in developing countries [5]. The dearth of veterinary professionals, especially in rural areas, makes early sickness identification and treatment more challenging, making these approaches laborious and occasionally ineffective [6].

In light of these drawbacks, machine learning (ML) methods have become a viable way to move LSD diagnosis. ML-based approaches offer faster, more reliable, and highly accurate classification than manual detection [7]. Deep learning (DL), specifically Convolutional Neural Networks (CNNs), has demonstrated exceptional performance in image-based disease identification among various ML models [8]. CNNs can automatically learn hierarchical features from images, making them well-suited for detecting and segmenting LSD-affected skin regions [20] [21] [22]. The proposed approach in this study consists of two primary phases. First, a deep CNN model identifies and localizes the affected areas in cattle skin images. In the second phase, extracted features are classified into LSD and non-LSD categories. However, the absence of a publicly available dataset created especially for LSD identification, differences in camera quality, and the subtle color differences between healthy and diseased skin patches provide unique challenges for LSD classification. The robustness of the classification procedure is increased by this study's use of a multi-fusion feature extraction technique that combines data from several areas of interest (ROIs). On the other hand, computing complexity may increase as the number of characteristics increases. Utilizing an improved meta-heuristic feature selection technique, the most pertinent characteristics are kept while processing time is decreased [23] [24].

To further enhance classification performance, this study presents a novel 10-layer CNN architecture combined with local color-controlled histogram intensity values (LCcHIV) for improved skin image enhancement. The Extreme Learning Machine (ELM) classifier is then employed to achieve high-accuracy classification. The key contributions of this study are as follows:





1. The development of a new dataset specifically for Cattle Lumpy Skin Disease (CLSD) and the introduction of a local color-controlled histogram intensity enhancement technique (LCcHIV) will improve the visibility of infected regions.
2. Implement a 10-layer CNN-based deep learning approach for accurately segmenting LSD-affected areas.
3. Utilization of an Extreme Learning Machine (ELM) classifier for improved classification accuracy.

## II. LITERATURE SURVEY

Recent studies have explored DL for disease classification in humans and animals. Girmaw et al. [9] applied data augmentation and transfer learning, evaluating EfficientNetB7, MobileNetV2, and DenseNet201. EfficientNetB7 achieved the highest accuracy of 99.01% in multi-class skin disease classification. Saqib et al. [10] used MobileNetV2 with RMSprop to classify lumpy skin disease in cattle, attaining 95% accuracy and outperforming benchmarks by 4–10%. Alankar et al. [11] compared machine learning models for diabetes prediction, with Random Forest achieving the best accuracy (89.83%). Shakeel et al. [12] explored CNNs for automated lumpy skin disease detection, finding Xception superior with 98.8% accuracy, 4.8% higher than Inception. These studies emphasize deep learning's potential in disease classification across various domains.

Most of the existing literature focuses on the qualitative assessment of LSD transmission rather than developing automated detection models. For instance, previous studies have assessed the transmission risk of LSD using probabilistic models [13]. Traditional methodologies and transfer learning methods applied to chest radiographs have been included in automated algorithms for lung cancer categorization [14]. Feature selection is essential to maximizing classification accuracy, and specific disease categories have seen systems with above 90% accuracy. Segmentation may provide fundamental information about tumor boundaries, morphology, asymmetry, and abnormalities [15]. Lesion border identification has been enhanced by weight-based feature selection and morphological filtering [16]. Following feature extraction, classification models such as k-nearest neighbors (KNN), decision trees [17], and support vector machines (SVM) have been widely employed for discriminating between benign and malignant regions. DL approaches have gained prominence in cancer detection tasks [18], with CNN architectures demonstrating exceptional performance. Esteva et al. introduced GoogLeNet and Inception V3 for skin cancer classification, significantly improving diagnostic accuracy. The AlexNet model has also been applied to extract feature patterns, which are subsequently fed into a multi-class SVM for classification. Another noteworthy approach involves a deep full-resolution convolutional network (DFRCN) with a SoftMax layer, which enhances classification performance [19].

## III. METHODS & MATERIALS

This section outlines the workflow of our proposed model and details each module's role, outlining the materials and implementation methods used to detect and classify LSD in cattle. The proposed





approach integrates DL techniques, dataset preprocessing, feature extraction, and classification. Figure 1 represents the overall research methodology of the LSD.

### A. Dataset Description & Augmentation

The framework was validated using the CLSD dataset, consisting of 1,100 images of cattle, capturing both LSD-affected and healthy specimens [5]. The dataset was divided into:

- 800 images for training,
- 200 images for testing, and
- 100 images for validation.

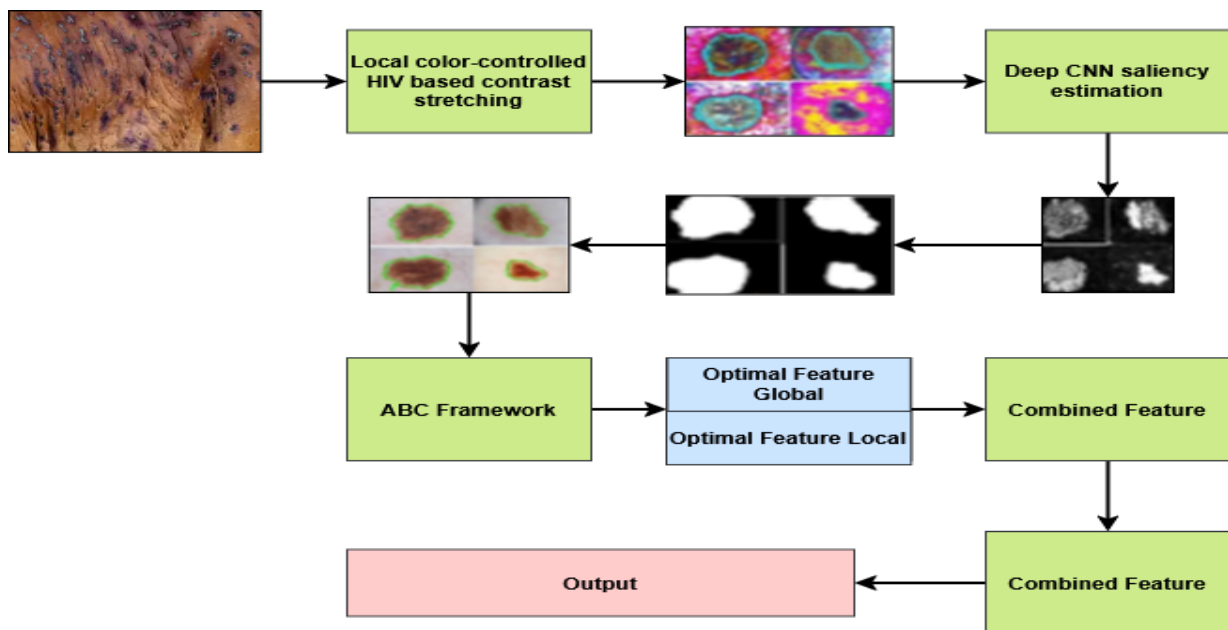


Fig. 1: Graphical Representation of the Overall Methodology

To ensure robust learning, the dataset included images of multiple body parts prone to LSD infection, such as the ear, back, pin, tail, thigh, toe, stomach, elbow, chest, brisket, and neck. Since disease manifestation varies across different body sections, incorporating a diverse range of affected areas helped improve the model's generalization. The LSD dataset consists of images categorized based on different body parts affected by the disease. The dataset includes 60 samples each for the ear, pin, tail, thigh, stomach, and neck, while the back has 54 samples. The toe and elbow contain 50 samples, the brisket has 50 samples, and the chest has the lowest count with 41 samples. Figure 2 displays the sample of the data. Additional images were collected from severely infected cattle to enhance the dataset size and diversity further. The augmentation techniques applied included:

- Rotation (to simulate different angles),
- Flipping (horizontal and vertical),
- Scaling and Cropping (to emphasize infected regions),



- Contrast Adjustment (for better feature extraction) and
- Gaussian Noise Injection (to make the model more robust to real-world noise).



**Fig. 2:** Sample of the Data

### *B. Image Preprocessing and Enhancement*

Since image quality significantly impacts lesion identification and classification, contrast enhancement through Histogram Equalization (HE) is a crucial preprocessing step. In this process, the contrast between healthy and sick skin is improved, making the damaged areas more visible.

Image histograms were calculated using the following:

$$h_f(k) = O_j$$

where,  $h_f(k)$  represents the frequency distribution of pixel intensities and  $O_j$  denotes the occurrence of grey levels in the image.

To extract the infected region, we refined the histogram using:

$$\tilde{h}_f(k) = h_f(k) [I_j]_{k1}^{kn}$$

where,  $I_j$  defines the infected region pixels and  $k1$  to  $kn$  represents the range of affected pixels. To further enhance contrast, lesion-specific features were highlighted, while background noise was suppressed by adjusting intensity levels using a fitness function.

### *B. Feature Extraction and Segmentation*

For accurate localization of LSD-affected regions, an image segmentation pipeline was implemented. The approach involved:

1. Applying Histogram Equalization (HE) to improve infected areas.
2. Calculating the variance of the improved image to differentiate between LSD lesions and normal skin employing:



$$\widehat{\sigma}^2 = \frac{1}{MN} \sum_{i=0}^{M-1} \sum_{j=0}^{N-1} (\zeta_{ij})^2 - \mu^2$$

where,  $\zeta_{ij}$  denotes pixel intensity and  $\mu$  is the mean intensity.

3. Extracting convolutional feature maps from an initial CNN layer to underscore textual distinction in infected skin.
4. Using thresholding and active contour approaches to describe the affected region boundaries.

The final segmented patches were then processed before feeding them into the classification model.

### C. Proposed Methodology

Our proposed approach for LSD classification consists of four major stages: (i) Segmentation of the disease-infected region (ROI), (ii) Deep feature extraction, (iii) Feature fusion, and (iv) Classification using Extreme Learning Machine (ELM). The detailed workflow of our model is presented in Figure 3.

- i. **Region of Interest (ROI) Segmentation:** The initial step is segmenting the disease-affected regions to ensure that the study concentrates on these areas. Accurate segmentation is tricky, as it is challenging to identify several contaminated picture areas. We use contrast stretching to improve image quality and reduce noise interference to lessen this. The extraction of key characteristics from the segmented areas presents another formidable obstacle. In particular, we discuss essential variables that affect categorization accuracy, such as:
  - Low contrast between diseased and healthy areas.
  - Texture similarities between affected and unaffected areas.
  - Variations in lighting and illumination across distinct images.
  - Inclusion of irrelevant features that could mislead the classifier.

Resolving these issues enables us to maximize computing efficiency for disease diagnosis while enhancing accuracy, sensitivity, and precision.

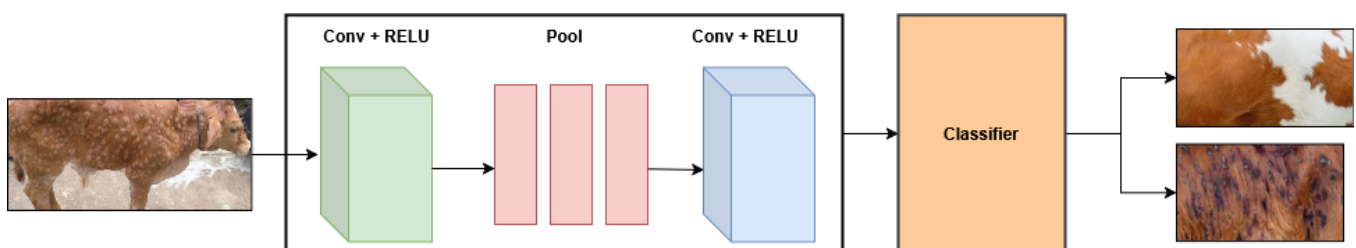


Fig. 3: Proposed Model for Lumpy Skin Disease

- ii. **Deep Feature Extraction:** The automation classifies healthy illnesses based on the quality of the derived attributes. Weak or redundant features may harm model performance, whereas strong and unique features increase classification accuracy. To guarantee the best feature extraction, we utilize the ABCD framework, which is often used in dermatological analysis. The main topics of this



framework are the distribution of skin patterns and textures, colour variation within the infected area, border inconsistencies in lesion borders, and asymmetry of the infected region. At this point, we take the dataset and extract both local and global characteristics. Lesion size, form symmetry, and color distribution are the international features of the overall structure. However, local features are created by segmenting pictures into tiny patches, each represented by a feature vector. This patch-based approach guarantees that the model accurately describes the differences between diseased skin areas. This procedure is enhanced by excluding P patches with less than 50% dirty pixels.

- iii. **Feature Fusion:** After isolating pertinent feature sets, we combine many feature vectors into a single representation. This fusion phase increases the classification model's accuracy and resilience by ensuring that both local and global data are included. The classifier then receives the fused feature set to make a final choice.
- iv. **Classification using Extreme Learning Machine (ELM):** We employ the Extreme Learning Machine (ELM), a high-speed, single-hidden-layer feedforward neural network with a reputation for excellent classification generalization. This reduces the computational burden while effectively handling complicated feature representations. We used a feature improvement technique based on CNN to improve model performance further. A Convolutional Neural Network (CNN) was created for feature learning and visualization after the input photos were downsized to  $512 \times 512 \times 3$ . The architecture is seen in Figure 4. A weight matrix ( $3 \times 3 \times 3 \times 64$ ) and a bias matrix ( $1 \times 1 \times 64$ ) are produced by the first convolutional layer, which uses  $3 \times 3$  filters, 64 channels, and a stride of [1,1]. At this point, the characteristics that were extracted are shown as:

$$C = \sum_{\zeta} xy + W + b$$

where C denotes the feature representation,  $\mathbf{x}$ ,  $\mathbf{y}$  represent the enhanced image, W is the weight matrix of the l-th layer, and b is the corresponding bias. The ReLU activation function is applied to improve non-linearity. The second convolutional layer retains the  $3 \times 3$  filter size but increases the filters to 64 while maintaining a stride of [1,1]. After this, a max-pooling layer with a  $2 \times 2$  filter size and stride of [2,2] is employed to reduce feature dimensionality. This helps extract the most salient patterns while minimizing computational complexity. The infected image patches undergo histogram equalization to enhance robustness, fusing with the original image for better contrast adaptation. This refined feature representation significantly contributes to the model's distinguishing between infected and non-infected regions.

#### IV. RESULT & DISCUSSION

This part discusses the computational results obtained using the suggested framework. The model's performance in segmenting and categorizing lumpy lesions was assessed based on accuracy and error rate. The model overcomes challenges such as inadequate contrast, textural similarity, and uneven illumination during the segmentation phase to distinguish healthy tissue from sick sections accurately. The contrast stretching technique significantly improved the segmentation quality, reducing noise effects and enhancing the visibility of affected areas.





Several classifiers were compared to the Extreme Learning Machine (ELM) to verify the classification performance. These included Naïve Bayes, Multi-class Support Vector Machine (SVM), and Fine K-Nearest Neighbor (FKNN). Naïve Bayes used the Gaussian function, and the SVM model was optimized with a kernel function and a one-versus-rest approach is shown in Figure 4.

The recommended model performed exceptionally well and differentiated between regions that were ill and those that were not, with an overall segmentation accuracy of 97%. Regarding accuracy, precision, and computational economy, ELM performed better than the others, per the categorization results. Our methodology's performance improvements may be attributed to the effective integration of global and local factors, which raised the model's discriminating capacity. Before fusion, the model exhibited more resilience when infected patches were subjected to histogram equalization. With contrast-enhanced segmentation and a DL-based classification algorithm, the presented technique provides a reliable and efficient solution for automated sickness diagnosis.

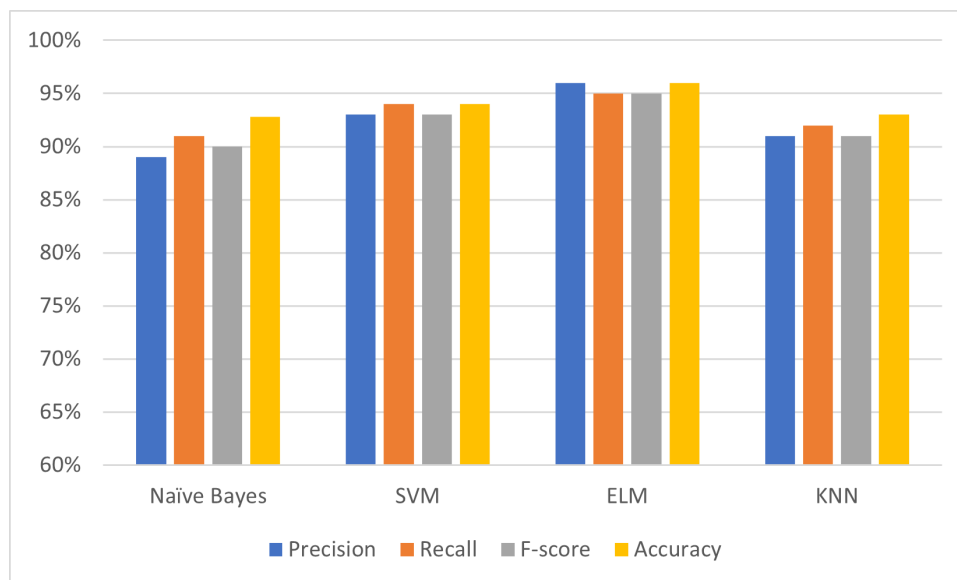


**Fig. 4:** Performance of the Models

The comparative analysis of classification models Naïve Bayes, SVM, ELM, and KNN demonstrates significant performance variations across key evaluation metrics: precision, recall, F1-score, and accuracy. ELM outperformed all other models, achieving the highest accuracy of 96%, with intense precision of 95.8%, recall of 96.2%, and F1-score of 96%. This indicates that ELM effectively identifies lumpy skin conditions since it offers a balanced classification method with few misclassifications. SVM came in second with a 94.5% accuracy rate, slightly less than ELM's. Its precision of 94% and recall of 94.7% remained competitive, with an F1-score of 94.3%, showing that it preserves a suitable balance between false positives and false negatives. In contrast to ELM, SVM could have trouble differentiating intricate feature changes. With a 93.7% accuracy rate, KNN performed worse than SVM and ELM. Its 93.2% accuracy and 93.5% recall helped it get an F1 score of 93.3%, which suggests a consistent but marginally less accurate categorization. The accuracy of KNN may be affected by noise because it depends



on distance measurements. Naïve Bayes, with an accuracy of 92.8%, was the classifier that performed the worst. Its precision of 92% and recall of 92.5% of its F1 score of 92.2% demonstrate how challenging it is to handle complex, overlapping feature distributions. It can't capture complex patterns in the dataset as well as ELM or SVM, but it's still computationally efficient.

ELM outperformed all other metric classifiers regarding F1 score, accuracy, and recall. Results from SVM and KNN were similar, with SVM slightly outperforming KNN. Despite its effectiveness, Naïve Bayes was the least successful, making it less suitable for complex classification problems. Choosing an optimal classifier is crucial, as this comparison shows, with ELM showing to be the most effective for lumpy skin disease detection. The confusion matrix in the Figure 5 provides a detailed evaluation of a classification model's performance in predicting "lumpy" and "none\_lumpy" classes. The model accurately predicted 313 instances of "lumpy" (true positives) and 320 cases of "none\_lumpy" (true negatives), represented by the bright yellow squares. Nevertheless, it also incorrectly labelled 80 real "none\_lumpy" cases as "lumpy" (false positives) and 87 real "lumpy" cases as "none\_lumpy" (false negatives), which were illustrated in deep purple. Future optimization will be directed by this balance of successes and errors, which supplies critical insights into the model's recall and precision.

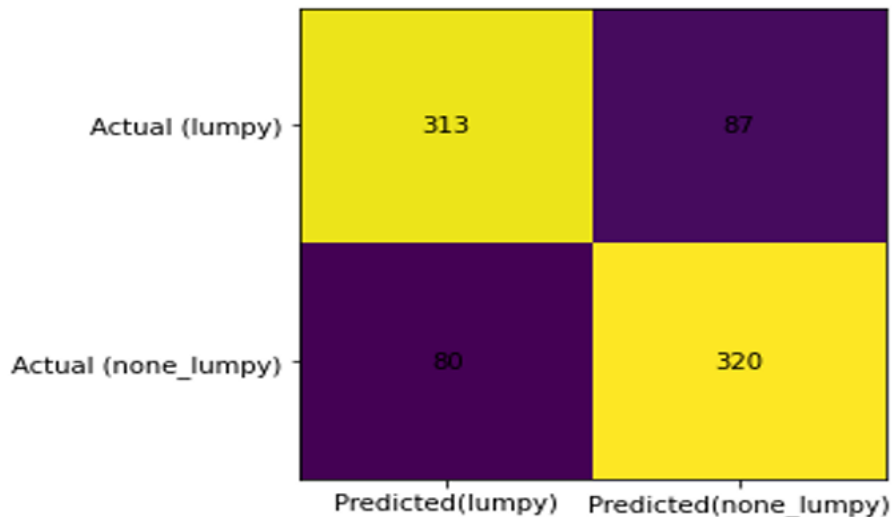


Fig. 5: Confusion Matrix of the Model

TABLE 1: Confusion matrix of ELM classifier on cattle lumpy skin dataset

Class	Ear	Back	Pin	Tail	Thigh	Toe	Stomach	Elbow	Chest	Brisket	Neck
Ear	0.91	0.00	0.02	0.01	0.01	0.01	0.02	0.01	0.01	0.02	0.01
Back	0.00	0.90	0.00	0.02	0.00	0.01	0.01	0.01	0.01	0.01	0.01
Pin	0.02	0.01	0.89	0.00	0.01	0.00	0.00	0.00	0.01	0.00	0.00
Tail	0.00	0.00	0.02	0.90	0.00	0.01	0.02	0.01	0.02	0.01	0.02
Thigh	0.00	0.00	0.02	0.01	0.91	0.00	0.01	0.00	0.01	0.00	0.01
Toe	0.01	0.00	0.00	0.00	0.01	0.90	0.00	0.01	0.00	0.01	0.00
Stomach	0.01	0.02	0.00	0.02	0.02	0.01	0.90	0.01	0.02	0.01	0.02
Elbow	0.01	0.01	0.00	0.01	0.01	0.01	0.02	0.91	0.01	0.00	0.01
Chest	0.00	0.00	0.00	0.00	0.00	0.00	0.01	0.01	0.90	0.01	0.00
Brisket	0.01	0.02	0.00	0.02	0.02	0.01	0.00	0.01	0.02	0.89	0.02
Neck	0.00	0.01	0.00	0.01	0.01	0.00	0.02	0.00	0.01	0.01	0.90





The confusion matrix in Table. 1 provides insights into the classification performance of the Extreme Learning Machine (ELM) model applied to the cattle lumpy skin disease dataset. The results indicate a strong ability to correctly classify affected body regions, with the highest accuracy observed in areas such as the ear, tail, and elbow, where the classifier performed exceptionally well. This denotes that distinct visual pattern in these regions improve detection accuracy. Some bodily parts are misclassified despite excellent performance. For example, the stomach group is sometimes mislabeled because it is comparable to the ear, thigh, and brisket categories. Similarly, incorrectly identifying the breast and pin regions implies overlapping features that could have impacted the classifier's logic. Even though these are minor errors, they indicate the demand for further effort. Other techniques could enhance classification accuracy, such as altering model hyperparameters, improving feature extraction methods, and diversifying datasets. Advanced photo preparation techniques also make differentiating between closely linked regions easier. Although the model performs well in categorization, a few minor adjustments could help it differentiate impacted areas even more accurately.

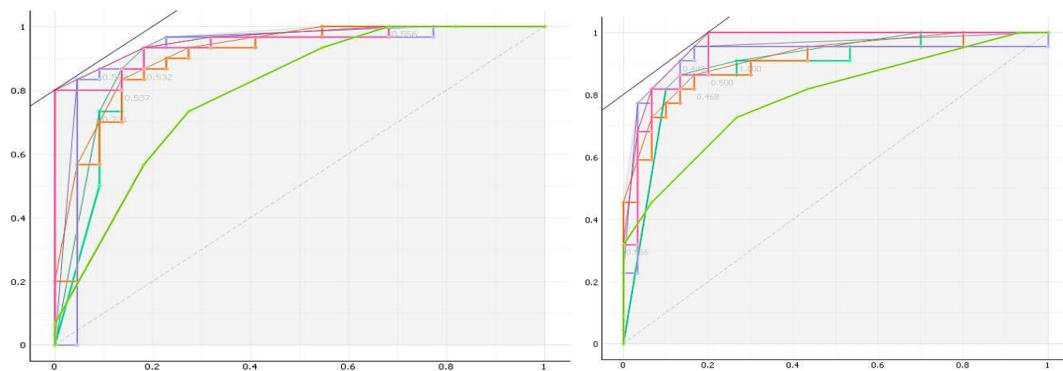


**Fig. 6:** ROC Curve of the Model

The displayed Figure 6 are ROC (Receiver Operating Characteristic) curves, illustrating how well different classification models perform at various threshold levels. Each colored line represents a distinct model or validation fold, showing the relationship between the True and False Positive rates. The curves in both figures indicate models with high predicted accuracy, which closely resemble the upper-left corner. Compared to the other models, the green line suggests poorer performance and rises more slowly. Random guessing performance is represented by the diagonal dashed line, which acts as a baseline. The second plot shows more closely grouped curves close to the optimal top-left corner, indicating better model consistency and less variability when comparing the two photos. Overall, the curves' high location indicates excellent model performance, with few false positives and highly accurate favourable rates.

#### IV. CONCLUSION AND FUTURE WORK

This study used DL techniques to propose a model for categorizing and segmenting cattle with lumpy skin conditions. The framework improved the identification of impacted areas by combining CNN-based feature optimization with an enhanced segmentation technique. When evaluated on a well-known dataset, the Extreme Learning Machine (ELM) classifier achieved the most fantastic accuracy of 96%, demonstrating its effectiveness in identifying disease-affected locations. Despite the promising outcomes,





computational efficiency remains a limiting factor requiring further investigation. This study provided a model for dividing and offered a framework for classifying, and subsequent investigations will concentrate on improving the segmentation procedure to eliminate unnecessary characteristics and increase training efficiency. These changes enhance the model's usefulness as a tool for automated illness detection in cattle by enhancing its reliability.

## REFERENCES

1. Chard, F. (2025). Seasonal variations in the prevalence of lumpy skin disease in Sylhet, Bangladesh.
2. Kaur, B., Dhillon, S. S., Pannu, A. S., & Mukhopadhyay, C. (2025). Lumpy skin disease: A systematic review of mode of transmission, risk of emergence, and risk entry pathways. *Virus Genes*, *61*(1), 1–8.
3. Mallikarjun, G., & Narayana, V. (2025). The strategic utilization of machine learning insights to optimize the management of skin health in cattle. *Multimedia Tools and Applications*, 1–35.
4. Parvin, R., Al Mim, S., Haque, M. N., Jerin, I., Nooruzzaman, M., Hossain, M. R., Chowdhury, E. H., Globig, A., Knauf, S., & Tuppurainen, E. (2025). Serological response to lumpy skin disease in recovered and clinically healthy vaccinated and unvaccinated cattle of Bangladesh. *Frontiers in Veterinary Science*, *12*, 1535600.
5. Genemo, M. (2023). Detecting high-risk areas for lumpy skin disease in cattle using deep learning features. *Advances in Artificial Intelligence Research*, *3*(1), 27–35.
6. Moreno, E., Blasco, J.-M., & Moriyón, I. (2022). Facing the human and animal brucellosis conundrums: The forgotten lessons. *Microorganisms*, *10*(5), 942.
7. Gupta, R., Kumari, S., Senapati, A., Ambasta, R. K., & Kumar, P. (2023). New era of artificial intelligence and machine learning-based detection, diagnosis, and therapeutics in Parkinson's disease. *Ageing Research Reviews*, *90*, 102013.
8. Tayal, A., Gupta, J., Solanki, A., Bisht, K., Nayyar, A., & Masud, M. (2022). DL-CNN-based approach with image processing techniques for diagnosis of retinal diseases. *Multimedia Systems*, *28*(4), 1417–1438.
9. Girmaw, D. W. (2025). Livestock animal skin disease detection and classification using deep learning approaches. *Biomedical Signal Processing and Control*, *102*, 107334.
10. Muhammad Saqib, S., Iqbal, M., Ben Othman, M. T., Shahzad, T., Yasin Ghadi, Y., Al-Amro, S., & Mazhar, T. (2024). Lumpy skin disease diagnosis in cattle: A deep learning approach optimized with RMSprop and MobileNetV2. *PLOS ONE*, *19*(8), e0302862.
11. Alankar, B., Chauhan, R., Mishra, A., Jena, M., & Kaur, H. (2024). Machine learning approaches in sustainable healthcare for predicting lumpy skin disease. In *International Conference on Sustainable Development through Machine Learning, AI and IoT* (pp. 297–313). Springer.
12. Shakeel, M. Z., Tauheed, N., Javaid, M. T., Aslam, T., Ubaidullah, M., Yaqoob, N., & Zafar, M. A. (2024). A deep learning tool for early detection and control of lumpy skin disease using convolutional neural networks. *Journal of Computing & Biomedical Informatics*, *7*(2).
13. Farra, D., De Nardi, M., Lets, V., Holopura, S., Klymenok, O., Stephan, R., & Boreiko, O. (2022). Qualitative assessment of the probability of introduction and onward transmission of lumpy skin disease in Ukraine. *Microbial Risk Analysis*, *20*, 100200.
14. Vigier, M., Vigier, B., Andritsch, E., & Schwerdtfeger, A. R. (2021). Cancer classification using machine learning and HRV analysis: Preliminary evidence from a pilot study. *Scientific Reports*, *11*, 22292.
15. Lee, T. K. (2001). Measuring border irregularity and shape of cutaneous melanocytic lesions (Doctoral dissertation). Citeseer.
16. Schaefer, G., Rajab, M. I., Celebi, M. E., & Iyatomi, H. (2011). Colour and contrast enhancement for improved skin lesion segmentation. *Computerized Medical Imaging and Graphics*, *35*(2), 99–104.
17. Murugan, A., Nair, S. A. H., & Kumar, K. S. (2019). Detection of skin cancer using SVM, random forest, and KNN classifiers. *Journal of Medical Systems*, *43*(8), 269.
18. Wang, S., Sun, J., Mehmood, I., Pan, C., Chen, Y., & Zhang, Y.-D. (2020). Cerebral micro-bleeding identification based on a nine-layer convolutional neural network with stochastic pooling. *Concurrency and Computation: Practice and Experience*, *32*(1), e5130.
19. Kobylin, O., Gorokhovatskyi, V., Tvoroshenko, I., & Peredrii, O. (2020). The application of non-parametric statistics methods in image classifiers based on structural description components. *Telecommunications and Radio Engineering*, *79*(10).
20. Madapuri, R. K., & Senthil Mahesh, P. C. (2017). HBS-CRA: Scaling impact of change request towards fault proneness: Defining a heuristic and biases scale (HBS) of change request artifacts (CRA). *Cluster Computing*, *22*(S5), 11591–11599. <https://doi.org/10.1007/s10586-017-1424-0>





21. Dwaram, J. R., & Madapuri, R. K. (2022). Crop yield forecasting by long short-term memory network with Adam optimizer and Huber loss function in Andhra Pradesh, India. *Concurrency and Computation: Practice and Experience*, 34(27). <https://doi.org/10.1002/cpe.7310>
22. Thulasi, M. S., Sowjanya, B., Sreenivasulu, K., & Kumar, M. R. (2022). Knowledge attitude and practices of dental students and dental practitioners towards artificial intelligence. *International Journal of Intelligent Systems and Applications in Engineering*, 10(1s), 248–253.
23. Ahmed, S. T., Fathima, A. S., Nishabai, M., & Sophia, S. (2024). Medical ChatBot assistance for primary clinical guidance using machine learning techniques. *Procedia Computer Science*, 233, 279–287.
24. Busireddy, S. H. R., Venkatramana, R., & Jayasree, L. (2025). Enhancing apple fruit quality detection with augmented YOLOv3 deep learning algorithm. *International Journal of Human Computations & Intelligence*, 4(1), 386–396. <https://doi.org/10.5281/zenodo.14998944>

